

# The Canadian Meteor Orbit Radar Meteor Stream Catalogue

Peter Brown · Robert J. Weryk · Daniel K. Wong · James Jones

Received: 30 June 2007 / Accepted: 25 September 2007 / Published online: 12 October 2007  
© Springer Science+Business Media B.V. 2007

**Abstract** The Canadian Meteor Orbit Radar is a multi-frequency backscatter radar which has been in routine operation since 1999, with an orbit measurement capability since 2002. In total, CMOR has measured over 2 million orbits of meteoroids with masses greater than 10  $\mu\text{g}$ , while recording more than 18 million meteor echoes in total. We have applied a two stage comparative technique for identifying meteor streams in this dataset by making use of clustering in radiant and velocities without employing orbital element comparisons directly. From the large dataset of single station echoes, combined radiant activity maps have been constructed by binning and then stacking each years data per degree of solar longitude. Using the single-station mapping technique described in Jones and Jones (Mon Not R Astron Soc 367:1050–1056, 2006) we have identified probable streams from these single station observations. Additionally, using individual radiant and velocity data from the multi-station velocity determination routines, we have utilized a wavelet search algorithm in radiant and velocity space to construct a list of probable streams. These two lists were then compared and only streams detected by both techniques, on multiple frequencies and in multiple years were assigned stream status. From this analysis we have identified 45 annual minor and major streams with high reliability.

**Keywords** Meteor streams · Radar · Meteoroids

## 1 Introduction

The recognition of meteor streams as debris from cometary activity stands as one of the seminal discoveries in meteor astronomy over the last two centuries (Burke 1986). Meteor streams trace the present and past activity of their parent bodies and therefore form an important link to understanding the dynamical and physical evolution of comets. Additionally, recognizing associations between streams and asteroids (the Geminids and 3200

---

P. Brown (✉) · R. J. Weryk · D. K. Wong · J. Jones  
Department of Physics and Astronomy, University of Western Ontario, London, ON, Canada N6A 3K7  
e-mail: pbrown@uwo.ca

Phaethon, the Quadrantids and 2003 EH1 for example) may provide insight into transition objects which straddle the comet—asteroid boundary.

The starting point for all stream studies is separating stream meteoroids, (which usually have a single common parentage), from the sporadic background; this implies associating individual meteoroid orbits with other meteoroid orbits. Historically this has been accomplished through use of a dissimilarity criterion employing orbital elements and/or radiant/velocity measurements of individual meteoroids (cf. Valsecchi et al. 1999; Jopek et al. (1999) and references therein). These various criteria (and associated critical limit) have been applied to a few distinct datasets where individual meteoroid orbits have been measured (such as the Harvard Super-Schmidt photographic data) in an effort to identify probable streams.

It is clear that such approaches work well in identifying the major streams; almost all the various dissimilarity criteria “extract” the dozen or so most active streams, though the particulars of period of activity, radiant location/drift may vary somewhat. Where significant differences arise, however, is in minor stream identification. Here earlier datasets might have only a few orbits and errors in these orbits make separation from the sporadic background problematic.

The solution to this problem is to perform searches on meteoroid orbit datasets which are large enough that the many minor streams are readily identifiable purely on statistical grounds. A recent attempt along these lines by Galligan and Baggaley (2002) identified half a dozen streams in the Advanced Meteor Orbit Radar (AMOR) collection of 0.5 million orbits. The small number of positive stream detections in the AMOR dataset is undoubtedly a function of the small particle sizes observed by AMOR ( $\sim 40 \mu\text{m}$ ), the sporadic background vastly outnumbering stream meteoroids at such small meteoroid sizes (cf. Jenniskens 2006). The technique and methodology used by Galligan and Baggaley (2002) forms the basis of the present work which applies a related technique to identification of meteor streams in the radar data collected by the Canadian Meteor Orbit Radar (CMOR).

## 2 Equipment and Data Collection Techniques

The CMOR (43.264 N, 80.772 W) is a triple frequency (17.45, 29.85 and 38.15 MHz) backscatter system with all three systems operating simultaneously at a pulse repetition frequency of 532 Hz and 6 kW peak transmit power. Each radar system has a receiving interferometry array which permits measurement of echo direction. The vertically directed transmit and receive antennae have a combined beam pattern which is nearly all-sky; the effective beamwidth to the 3 dB points is located  $45^\circ$  from the zenith. The 29.85 MHz unit also has two outlying stations connected to the main site via UHF datalinks. These outlying stations record reflections from points along some meteor trails distant from the main site specular reflection point. Combining the relative timing of the detections from these two remote sites relative to the main site and the interferometric information permits a complete reconstruction of the meteor velocity vector. Additional details of the system and the data collection architecture are described in more detail in Jones et al. (2005) and Webster et al. (2004).

The radar is effectively sensitive to meteors with apparent radio magnitudes (cf. McKinley 1961)  $\sim +8$ . Figure 1 shows the distribution of apparent magnitudes and masses (as determined from the mass-magnitude-velocity relation of Verniani (1973)) for all meteoroids with determined orbits. The mean magnitude for echoes with measured

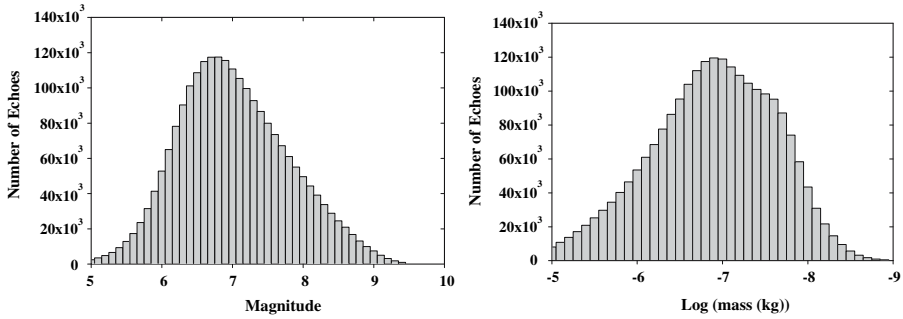


**Fig. 1** Magnitude distribution (left) and mass distribution (right) for all CMOR echoes having determined orbits

orbits is +7 and the mean mass is  $1.3 \times 10^{-7}$  kg; this is a lower limit as in the radar analysis it is assumed that the radar reflection specular point for any particular meteor ionization train coincides with the point of maximum ionization.

### 3 Errors and Biases

The detection of stream structure in CMOR data requires measurement of an interferometric location (altitude and azimuth of reflected RF pulse) for a given echo and an echo time. This information, together with the station location is sufficient to perform single station radiant mapping in equatorial coordinates (cf. Jones and Jones 2006). In addition to these data, two time-of-flight measurements from the outlying station on 29.85 MHz are needed to uniquely define a velocity vector for individual meteor echoes.

Errors in time of echo occurrence are essentially negligible, having precisions of order ms and accuracies  $<1$  s respectively. Interferometric errors are less than  $1^\circ$  for echoes with elevations above  $20^\circ$  (Jones et al. 1998). Since the interferometric error increases rapidly below this elevation, only echoes with elevations greater than  $20^\circ$  are used. Specifically, a mean error value in the interferometry  $<0.3^\circ$  was determined by Jones et al. (1998) through simulations using signal-to-noise ratios above 20 dB. From an analysis of single station radiants, Jones and Jones (2006) concluded that the effective spread in radiant positions due to interferometry errors was  $\sim 1.2^\circ$ . Finally, a direct comparison between simultaneously detected electro-optical meteors and radar echoes determined a mean error  $<0.2^\circ$  for echoes with elevations above  $50^\circ$  (Weryk and Brown 2007). The random errors in directionality are the main source of uncertainty; comparison between directions determined between 29 and 38 MHz yield a mean and median systematic difference in echo directions of  $<0.1^\circ$ . This is consistent with the observation that the receiver phases on all three systems drift by no more than  $0.7^\circ$  in a given day based on twice hourly automatic measurements over many years, with the mean drift  $<0.3^\circ$  throughout much of the year. This is a consequence of the temperature compensation employed for the radar systems, which ensures the hardware experience diurnal temperature variations  $<2^\circ\text{C}$  throughout most of the year.

For individual orbit measurements, the primary source of error in velocity and radiant measurement is in the estimation of the difference in time of occurrence between the remote sites and the main site. Typically this amounts to 1–2 pulses (1.9–3.8 ms).

However, slower meteoroids have much shallower rise times often resulting in larger absolute time errors (cf. Jones et al. 2005 for details of the time pick algorithm). This is partially compensated by the lower velocity (and hence longer time delays between the stations)—the opposite situation exists for faster meteoroids such that the relative error remains approximately constant as a function of velocity. The resulting errors amount to 5–10% in velocity and 1–2° in radiant direction. These error margins have been independently validated through comparison between simultaneously observed optical and radar events (Weryk and Brown 2007) which show even smaller differences, but apply on average to higher SNR echoes. The dependence of the actual error with SNR is still to be investigated with these simultaneous measurements.

Finally, we note that showers with high velocity meteoroids or with steep mass distribution indices (i.e. a preponderance of small meteoroids) will be more difficult to detect due to the effects of the echo height ceiling. Similarly, very slow streams will be selected against due to the high velocity dependence of ionization (cf. Ceplecha et al. 1998). Our all-sky coverage tends to limit the biases introduced by the beam pattern to purely declination effects. Radiants at high declinations have larger daily integrated collecting areas than those at low declinations (cf. Campbell-Brown and Jones 2006). For all the stream detections which follow we have not corrected for this declination sensitivity—in a future paper concerned solely with stream activity this collecting area bias will be examined in detail.

The single largest remaining systematic uncertainty in our measurements is  $V_\infty$ , the velocity at the top of the atmosphere. Our measurement of in-atmosphere velocity is subject to the effects of deceleration. For a particular echo this will be a function of the height at which our velocity measurement is made. Brown et al. (2005) have presented an empirical method of correcting CMOR data for height-deceleration effects as a function of velocity, but this relies on use of previous video/photographic estimates of stream  $V_\infty$  as a means of calibration. Thus our velocity estimates for the 11 streams used in the calibration are not strictly independent measurements. The streams used for calibration are listed in the summary stream table (Table 1).

#### 4 Stream Detection Methodology and Analysis

Detection of streams in CMOR data was performed as a two stage process. Each quasi-independent stage produced a list of possible radiants and a final master list was constructed from only streams which were detectable with both techniques, generally having comparable radiant locations and radiant drifts as determined by the two methods providing sufficient numbers of echoes were available for each technique.

In the first stage, all single station echoes on all three frequencies were combined into individual solar longitude bins from all years of observations. In total, 26.3, 18.3 and 11.0 million echoes were recorded on 17, 29 and 38 MHz systems respectively. This produces an equivalent single solar year, the assumption being that the streams of interest are active from the same radiant positions each year. Each solar longitude bin is then processed using the convolution technique described in Jones and Jones (2006). The result for each degree of solar longitude is a map of the relative radiant activity in equatorial coordinates. The relative radiant activity (or relative strength) quantifies local enhancement in the number density of echo radiants over size scales of 1–2° following the procedure outlined in Jones and Jones (2006). By examining several strong, known streams near the tails of their activity period, we determined a cutoff value in the scaled radiant activity

**Table 1** Stream list. Single station values and WC (wavelet coefficient analysis) are shown, together with geocentric radiant coordinates at the time of WC maximum. Streams highlighted in bold have been used as calibrations to compute a mean deceleration correction. Only showers having  $W_c$  in at least a single degree bin in solar longitude more than 10r above background are included in this compilation

Stream name	Single station analysis					Wavelet analysis					$\sigma V_g$ (km/s)									
	$\lambda_{max}$	$\lambda_{start}$	$\lambda_{end}$	Relative activity	$\Delta z$	$\pm \Delta z$	$\Delta \delta$	$\pm \Delta \delta$	$W_{c\ max}$	$\Delta z$		$\pm \Delta z$	$\Delta \delta$	$\pm \Delta \delta$	$\alpha_{max}$ (J2000)	$\delta_{max}$ (J2000)	$V_g$ (km/s)			
<b>April Lyrids</b>	<b>32.5</b>	<b>30</b>	<b>34</b>	<b>36</b>	<b>0.78</b>	<b>0.16</b>	<b>-0.42</b>	<b>0.21</b>	<b>32.5</b>	<b>31</b>	<b>33</b>	<b>26.8</b>	<b>1.50</b>	<b>0.06</b>	<b>-0.30</b>	<b>0.06</b>	<b>272.3</b>	<b>32.6</b>	<b>47.3</b>	<b>4.1</b>
Daytime April Piscids	32.5	30	36	26	0.90	0.08	0.37	0.05	24.5	16	33	18.1	0.90	0.04	0.39	0.03	3.8	5.5	28.9	3.4
<b>Eta Aquarids</b>	<b>44.5</b>	<b>33</b>	<b>64</b>	<b>277</b>	<b>0.69</b>	<b>0.01</b>	<b>0.33</b>	<b>0.01</b>	<b>45.5</b>	<b>35</b>	<b>59</b>	<b>285.2</b>	<b>0.69</b>	<b>0.01</b>	<b>0.33</b>	<b>0.00</b>	<b>338.0</b>	<b>-0.7</b>	<b>64.6</b>	<b>6.2</b>
Southern Daytime May Arietids	47.5	30	61	30	0.97	0.03	0.30	0.02	46.5	23	63	23.6	0.92	0.01	0.32	0.01	28.4	7.7	28.3	3.3
Northern Daytime omega Cetids	47.5	30	59	29	0.97	0.03	0.31	0.01	45.5	16	58	38.4	0.95	0.01	0.36	0.01	9.0	17.3	36.8	4.1
Southern Daytime omega Cetids	49.5	34	59	32	0.90	0.03	0.43	0.02	45.5	18	62	42.5	0.93	0.01	0.44	0.01	20.5	-6.1	36.9	3.9
<b>Daytime Arietids</b>	<b>76.5</b>	<b>65</b>	<b>93</b>	<b>255</b>	<b>0.63</b>	<b>0.02</b>	<b>0.19</b>	<b>0.01</b>	<b>74.5</b>	<b>64</b>	<b>88</b>	<b>169.8</b>	<b>0.60</b>	<b>0.02</b>	<b>0.19</b>	<b>0.01</b>	<b>41.7</b>	<b>23.6</b>	<b>39.1</b>	<b>4.2</b>
Daytime Zeta Perseids	83.5	47	95	41	1.01	0.02	0.25	0.01	74.5	58	88	32.0	1.00	0.02	0.20	0.01	57.4	23.4	26.4	3.9
Southern June Aquilids	80.5	78	81	28	-0.25	0.34	0.46	0.16	80.5	78	82	31.1	0.02	0.23	0.30	0.12	304.7	-32.8	38.6	3.4
Daytime Gamma Taurids	81.5	77	93	32	0.82	0.11	0.34	0.04	85.5	70	98	19.2	0.82	0.02	0.27	0.01	56.7	11.5	36.4	3.7
Daytime Epsilon Perseids	95.5	92	107	24	0.77	0.08	0.42	0.06	95.5	92	107	13.0	0.78	0.05	0.15	0.04	58.2	37.9	44.8	4.4
Daytime Beta Taurids	96.5	82	103	45	0.88	0.07	0.05	0.01	93.5	90	100	25.8	0.89	0.08	0.04	0.05	82.0	20.0	27.4	3.1
Vulpeculids	106.5	104	109	22	0.60	0.21	-0.36	0.26	106	104	106	17.2	1.50	0.40	0.45	0.38	326.3	14.7	29.9	3.2
Northern June Aquilids	108.5	85	114	29	0.81	0.02	0.20	0.02	102	77	117	44.8	0.83	0.01	0.16	0.01	310.4	-4.9	38.4	3.9

**Table 1** continued

Stream name	Single station analysis						Wavelet analysis													
	$\lambda_{\max}$	$\lambda_{\text{start}}$	$\lambda_{\text{end}}$	Relative activity	$\Delta z$	$\pm\Delta z$	$\Delta\delta$	$\pm\Delta\delta$	$\lambda_{\max}$	$\lambda_{\text{start}}$	$\lambda_{\text{end}}$	$W_{c,\max}$	$\Delta z$	$\pm\Delta z$	$\Delta\delta$	$\pm\Delta\delta$	$\alpha_{\max}$ (J2000)	$\delta_{\max}$ (J2000)	$V_g$ (km/s)	$\sigma V_g$ (km/s)
Beta Equuleids	108.5	104	113	20	0.84	0.18	-0.45	0.19	107	104	112	16.4	0.69	0.09	-0.28	0.14	321.5	8.7	31.6	3.1
July Sigma Cassiopeids	110.5	100	113	25	0.95	0.24	0.37	0.11	105.5	102	110	13.9	0.70	0.19	0.37	0.07	343	49.6	38.9	3.3
Psi Cassiopeids	116.5	112	120	27	0.62	0.26	0.68	0.18	118	110	124	22.1	1.22	0.15	0.43	0.06	11.9	65.4	44	4.6
<b>Alpha Capricornids</b>	<b>124.5</b>	<b>102</b>	<b>130</b>	<b>36</b>	<b>0.69</b>	<b>0.02</b>	<b>0.24</b>	<b>0.01</b>	<b>124</b>	<b>116</b>	<b>128</b>	<b>19.9</b>	<b>0.66</b>	<b>0.02</b>	<b>0.28</b>	<b>0.02</b>	<b>302.9</b>	<b>-9.9</b>	<b>22.2</b>	<b>2.3</b>
<b>Southern Delta Aquariids</b>	<b>125.5</b>	<b>115</b>	<b>155</b>	<b>356</b>	<b>0.77</b>	<b>0.01</b>	<b>0.28</b>	<b>0.01</b>	<b>127</b>	<b>115</b>	<b>145</b>	<b>342.4</b>	<b>0.78</b>	<b>0.01</b>	<b>0.25</b>	<b>0.01</b>	<b>341.0</b>	<b>-16.1</b>	<b>41.1</b>	<b>3.8</b>
Piscis Austrinids	125.5	121	138	26	0.53	0.10	0.17	0.06	126.5	125	131	11.0	0.89	0.09	0.16	0.09	347.9	-23.7	44.1	3.7
Southern Iota Aquariids	129.5	125	149	22	0.93	0.05	0.34	0.02	129.5	128	133	11.5	0.36	0.12	-0.14	0.07	332.9	-14.7	30.5	3.1
Daytime Xi Orionids	131.5	116	138	19	0.81	0.06	-0.09	0.03	131.5	131	133	6.5	0.90	NA	-0.40	NA	102.9	16.6	45.4	4.2
Northern Delta Aquariids	137.5	131	159	22	0.70	0.03	0.33	0.01	139	128	155	19.7	0.75	0.03	0.28	0.02	344.9	2.2	37.7	4.3
Perseids	139.5	123	142	103	1.35	0.07	0.23	0.02	140	134	142	74.5	1.23	0.09	0.27	0.07	46.9	56.9	62.1	7.2
Northern Iota Aquariids	167.5	113	182	33	0.84	0.01	0.33	0.01	160	145	176	18.8	0.80	0.02	0.33	0.02	356.0	3.0	28.6	3.6
Daytime Kappa Leonids	178.5	164	189	40	0.63	0.03	-0.31	0.02	183	171	193	21.7	0.55	0.02	-0.26	0.02	161.5	15.4	43.3	4.5
<b>Daytime Sextantids</b>	<b>187.5</b>	<b>180</b>	<b>193</b>	<b>83</b>	<b>0.69</b>	<b>0.02</b>	<b>-0.58</b>	<b>0.02</b>	<b>187</b>	<b>174</b>	<b>194</b>	<b>61.9</b>	<b>0.70</b>	<b>0.03</b>	<b>-0.51</b>	<b>0.01</b>	<b>154.6</b>	<b>-1.4</b>	<b>31.84</b>	<b>3.3</b>
<b>Southern Taurids</b>	<b>191.5</b>	<b>166</b>	<b>236</b>	<b>56</b>	<b>0.82</b>	<b>0.01</b>	<b>0.25</b>	<b>0.01</b>	<b>197</b>	<b>172</b>	<b>218</b>	<b>49.9</b>	<b>0.82</b>	<b>0.01</b>	<b>0.29</b>	<b>0.01</b>	<b>31.0</b>	<b>8.0</b>	<b>27.92</b>	<b>3.7</b>
October Draconids	195.5	195	195	20	0.00	0.00	0.00	0.00	196	195	195	24.4	0.00	0.00	0.00	0.00	261.7	54.8	19.7	2.3

**Table 1** continued

Stream name	Single station analysis						Wavelet analysis													
	$\lambda_{\max}$	$\lambda_{\text{start}}$	$\lambda_{\text{end}}$	Relative activity	$\Delta z$	$\pm\Delta z$	$\Delta\delta$	$\pm\Delta\delta$	$\lambda_{\max}$	$\lambda_{\text{start}}$	$\lambda_{\text{end}}$	$W_c$	$\Delta z$	$\pm\Delta z$	$\Delta\delta$	$\pm\Delta\delta$	$\alpha_{\max}$ (J2000)	$\delta_{\max}$ (J2000)	$V_g$ (km/s)	$\sigma V_g$ (km/s)
<b>Orionids</b>	<b>209.5</b>	<b>196</b>	<b>222</b>	<b>132</b>	<b>0.84</b>	<b>0.02</b>	<b>0.03</b>	<b>0.01</b>	<b>208</b>	<b>198</b>	<b>221</b>	<b>96.3</b>	<b>0.78</b>	<b>0.01</b>	<b>0.03</b>	<b>0.01</b>	<b>94.7</b>	<b>15.5</b>	<b>66.4</b>	<b>6.3</b>
Northern Taurids	223.5	201	236	31	0.90	0.02	0.24	0.01	225	207	235	21.9	0.88	0.01	0.19	0.02	53.3	21.0	28.1	2.9
<b>Leonids</b>	<b>236.5</b>	<b>230</b>	<b>238</b>	<b>82</b>	<b>0.51</b>	<b>0.15</b>	<b>-0.48</b>	<b>0.14</b>	<b>237</b>	<b>228</b>	<b>238</b>	<b>29.2</b>	<b>0.63</b>	<b>0.08</b>	<b>-0.27</b>	<b>0.06</b>	<b>155.0</b>	<b>21.6</b>	<b>69</b>	<b>6.8</b>
November omega Orionids	247.5	226	256	78	0.74	0.01	-0.02	0.01	246	230	253	63.9	0.74	0.02	-0.06	0.01	90.2	15.5	43.5	3.9
<b>Geminids</b>	<b>260.5</b>	<b>243</b>	<b>269</b>	<b>817</b>	<b>1.12</b>	<b>0.01</b>	<b>-0.16</b>	<b>0.01</b>	<b>262</b>	<b>244</b>	<b>267</b>	<b>568.0</b>	<b>1.10</b>	<b>0.02</b>	<b>0.17</b>	<b>0.02</b>	<b>112.8</b>	<b>32.1</b>	<b>35</b>	<b>3.8</b>
December Monocerotids	262.5	253	266	21	0.53	0.06	-0.05	0.05	262	252	264	21.3	0.63	0.03	-0.11	0.05	102.6	8.1	41.5	3.7
Ursids	270.5	270	270	29	0.00	0.00	0.00	0.00	271	270	270	39.5	0.00	0.00	0.00	0.00	222.0	74.6	37.6	5.1
Sigma Serpentids	275.5	271	282	18	0.74	0.08	-0.16	0.11	276	261	279	26.0	0.75	0.02	-0.14	0.03	242.8	-0.1	42.67	4
January Leonids	280.5	278	284	42	0.99	0.10	-0.36	0.03	283	280	284	37.6	0.66	0.11	-0.14	0.05	148.3	23.9	52.7	4.4
Omega Serpentids	280.5	270	281	25	0.60	0.06	0.08	0.10	275.5	271	279	16.5	0.76	0.05	0.11	0.18	242.7	0.5	38.9	3.4
<b>Quadrantids</b>	<b>283.5</b>	<b>281</b>	<b>286</b>	<b>238</b>	<b>-0.01</b>	<b>0.32</b>	<b>0.38</b>	<b>0.32</b>	<b>284</b>	<b>279</b>	<b>285</b>	<b>237.5</b>	<b>0.72</b>	<b>0.05</b>	<b>-0.55</b>	<b>0.23</b>	<b>231.7</b>	<b>48.5</b>	<b>42</b>	<b>4</b>
Alpha Cettids	290.5	280	294	17	0.69	0.05	-0.19	0.03	285.5	281	289	15.6	0.65	0.07	-0.17	0.06	127.6	-7.9	43.6	3.9
Theta Coronae Borealis	296.5	294	300	24	1.57	0.17	-0.91	0.11	297	293	303	63.2	0.70	0.16	-0.06	0.09	232.3	35.8	38.66	4.5
Lambda Bootids	295.5	283	299	27	1.36	0.13	-0.62	0.05	296	285	297	34.4	0.88	0.08	-0.69	0.03	219.6	43.2	41.75	4.2
Zeta Coronae Borealis	295.5	291	303	18	0.69	0.15	0.05	0.11	295	291	303	23.0	0.69	0.09	-0.11	0.08	244.8	31.1	44.25	4.3
Alpha Antilids	313.5	308	321	24	0.91	0.05	-0.38	0.06	316	299	320	30.7	0.84	0.03	-0.36	0.03	162.7	-12.6	44.75	4.3

corresponding to the average sporadic background which could be reliably used to separate noise from stream signals. This cutoff (15) was then used throughout the single station analysis. Figure 2 shows the maximum scaled radiant activity for each solar longitude degree with streams identified.

For each degree of solar longitude, all radiants above the threshold value are recorded. Finally, a potential list of streams is computed taking local maxima found from this single station mapping and comparing it to solar longitude bins before and after each interval. If additional local radiant maxima are found within  $\pm 2^\circ$  in right ascension and declination per degree solar longitude from the original solar longitude bin the individual maxima are linked and recorded as a possible stream. Linkages lasting more than three consecutive degrees and/or having maxima above 20 lasting at least two bins were then automatically identified. From this list, potential streams showing consistent radiant drifts in  $\alpha, \delta$  were saved and then manually examined to further reduce false detections. Cross-comparisons were made among the three frequencies with the requirement that 29 and 38 MHz show consistent radiant positions and radiant drifts for a stream to be recognized. Data from 17 MHz suffers from terrestrial broadcast interference during the day and hence the radiant maps from 17 MHz were used only as a backup means of confirmation not a primary selection filter. This procedure rapidly identified most major streams previously recorded in other lists as well as some new streams/minor streams.

In the second detection stage, all individual geocentric radiants measured using the time-of-flight technique on 29.85 MHz were examined separately for potential clustering. In total 2.5 million orbits were available for this stage of the analysis. The geocentric radiant locations and geocentric velocity of the orbit of each meteor together with the time of occurrence were used to detect enhancements relative to the sporadic background.

The identification of streams in this second stage was done by performing a wavelet transform on the geocentric radiant data. These data were further partitioned by geocentric velocity in bins corresponding approximately to the upper limit of the average error values in velocity (10%). Our searches were conducted across these velocity bins with varying probe sizes, the probe sizes representing the angular scale size of the wavelet probe (the

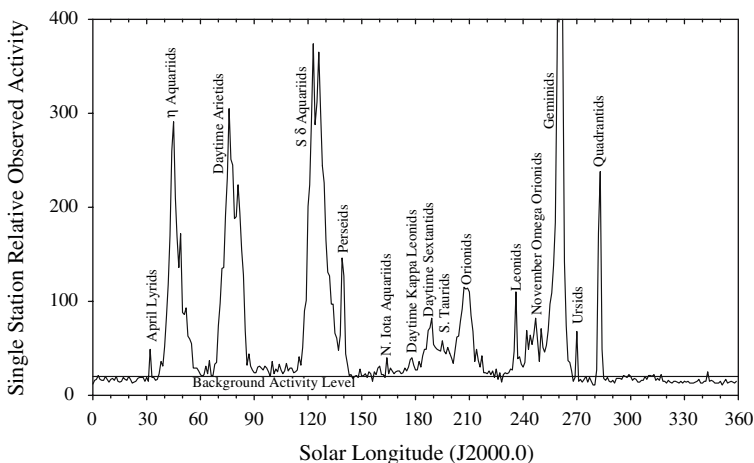


**Fig. 2** The maximum in single station radiant activity for each degree of solar longitude throughout the year. Prominent streams (activity above background as defined in the text) are marked



clustering size scale the particular probe is most sensitive). The wavelet transform and its application to radar meteor data is described in Galligan and Baggaley (2002).

We proceed by computing wavelet coefficients in a grid made up of  $0.5^\circ$  increments in sun-centred ecliptic longitude ( $\lambda - \lambda_o$ ) and latitude ( $\beta$ ). We use discrete wavelet probe sizes of 1, 2, 3, 4 and  $8^\circ$  and with geocentric velocity partitions from 14–75 km/s, spaced with bin intervals of 10% in speed. These combinations of wavelet coefficients are computed for each degree of solar longitude, with all meteoroid orbits from all years combined. Each degree of solar longitude has on average 12,000 individual radiant measurements.

For each wavelet grid location ( $\lambda - \lambda_o, \beta$ ) within a given probe size and velocity combination, the median and standard deviation of that particular grid point is computed over all degrees of solar longitude. Points more than  $3\sigma$  above the median are discarded and the process iteratively repeated until no more points forming the median at that grid location lie outside the  $3\sigma$  bounds. Local maxima in wavelet coefficients are then identified as those points more than  $3\sigma$  above the final median estimate and where the density of radiants is above a minimum threshold, which was empirically determined to be 20 radiant points per square degree.

These local maxima are then linked across individual solar longitude bins, provided the local maxima in adjacent solar longitude bins are separated by less than  $2.5^\circ$  in grid space or less than  $3.5^\circ$  if separated by two degrees of solar longitude. These potential streams are then further refined by requiring that at least one of the local maxima is  $>10\sigma$  above the median background. Single radiant points visible for only one solar longitude bin were considered potential streams if the local maxima was  $15\sigma$  above the median background.

With all these chains identified in solar longitude, velocity, probe size partitions, many duplicate potential streams appeared. Having identified the location in grid space where the potential radiants are located, the solar longitude bin of the stream maximum was then identified and wavelet coefficients computed in 1 km/s steps centred at the grid location maximum. It was found that the velocity bin where the maximum relative wavelet coefficient was determined was generally insensitive to medium-scale probe sizes (2, 3, 4 $^\circ$ ). The process of selecting a best-fit velocity and separation of the stream from the background in this manner is shown in Fig. 3a and b for the S. Delta Aquariid stream.

Once the best fit velocity bin was identified, the same procedure was applied in the solar longitude bin of the maximum (partitioned at the wavelet bin closest to the peak velocity) and different probe sizes from 0.1 to  $20^\circ$  at  $0.1^\circ$  intervals applied at the grid point maximum. The resulting curve identified the best fit probe size as the probe-size where the maximum wavelet coefficient was computed. This process is shown in Fig. 4 for the S. Delta Aquariid stream.

Once all potential stream chains were identified by this procedure, they were checked additionally for positive daily mean radiant drift in  $\alpha$  and consistent drifts for all points in both  $\alpha, \delta$ .

## 5 Results and Conclusions

A total of 45 streams were identified using the above described search criteria. Table 1 lists the stream names, period of detectable activity based on our criteria (for both single station and wavelet transformed data), radiant positions and radiant drifts and best-fit geocentric velocity. The errors are 1  $\sigma$  bounds for the velocity fits and for the linear regression in  $\alpha, \delta$ .

**Fig. 3** (a) (top): Wavelet coefficients (WC) in 1 km/s velocity steps partitioned for a probe size of  $3^\circ$  centred at the radiant at the time of maximum for the S.  $\delta$  Aquariid stream. The fit is Gaussian with a peak at 41.1 km/s and standard deviation of 3.8 km/s. (b) (below): Wavelet coefficients at a probe size of  $3^\circ$  for velocities between 39 and 45 km/s at the sun-centred grid coordinates of the maximum of the S.  $\delta$  Aquariid stream computed for each degree of solar longitude. Here the  $3\sigma$  detection threshold is at a WC of 5.3

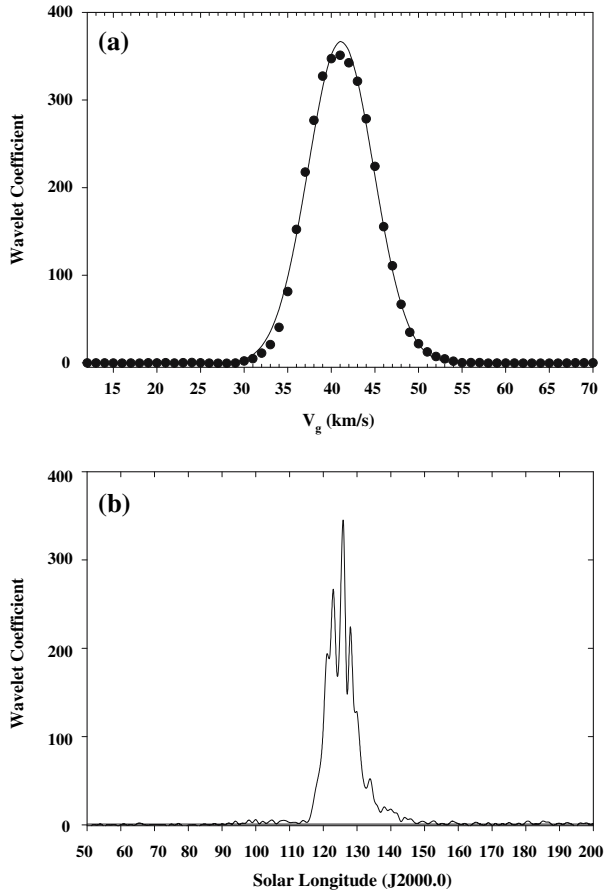
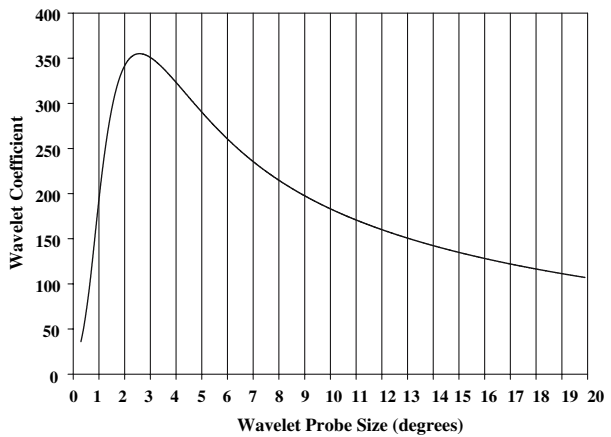


**Fig. 4** Wavelet coefficients as a function of probe size for velocities between 39 and 45 km/s at the sun-centred grid coordinates of the maximum of the S.  $\delta$  Aquariid stream on the day of maximum ( $\lambda_o = 126^\circ$ )



Note that for several streams a higher order fit is clearly needed for the radiant drift in  $\alpha, \delta$  (such as the Taurids and S. Delta Aquariids). However, we apply linear fits for ease of comparison with other literature sources.

A good portion (73%) of our detected streams have been previously described in the literature. A total of 12 of our 45 detected streams are unreported in the literature or have weak associations to previously poorly characterized streams making associations difficult.

In comparing the present list to previous primary data source stream lists, it is apparent that many individual streams have previously been detected or classified as multiple streams, when in fact the present work suggests they have a single stream origin. This is the result of the intermittent periods of coverage for many earlier surveys (particularly radar surveys), which often required manual operation. We also note that the relatively small number of stream detections as compared to the large number recognized by the IAU working list suggests either many streams have shallow mass distribution indices and are not highly populated at the smaller masses detectable by the radar or that the streams do not exist.

A more complete description of the CMOR meteor stream working list, together with detailed orbital data (and orbital element variations) as well as a more detailed analysis of the various streams from our data will appear separately. We also intend to examine the flux and mass distribution indices for all streams reported here. Relaxation of the relatively strict stream selection criteria applied here, (particularly for wavelet analysis), results in significantly more (almost double) the number of identified streams. Together with the increasing number of CMOR orbits (now more than 3 million) we expect to significantly increase our signal-to-noise detection thresholds for minor streams in the future.

**Acknowledgments** PGB thanks the Natural Sciences and Engineering Research Council, the Canada Research Chairs program and the Meteoroid Environment Office of NASA for funding support. J. Baggaley and an anonymous reviewer provided helpful comments to the first version of this manuscript.

## References

- J.G. Burke, *Cosmic Debris: Meteorites in History*. (University of California Press, Berkeley, 1986)  
P.G. Brown, J. Jones, R.J. Weryk, M.D. Campbell-Brown, *Earth Moon Planets* **95**, 617–626 (2005)  
M.D. Campbell-Brown, J. Jones, *Mon. Not. R. Astron. Soc.* **367**, 709–716 (2006)  
Z. Ceplecha, et al., *Space Sci. Rev.* **84**, 327–471 (1998)  
D.P. Galligan, J. Baggaley, in *Dust in the Solar System and Other Planetary Systems, Proc. IAU Colloq. 181.*, eds. by S.F. Green, I.P. Williams, J.A.M. McDonnell, N. McBride (Pergamon, Oxford, 2002), pp. 42–47  
P.J. Jenniskens, *Meteor Streams and Their Parent Comets*. (Cambridge University Press, 2006)  
J. Jones, P. Brown, K.J. Ellis, A.R. Webster, M.D. Campbell-Brown, Z. Krzemenski, R.J. Weryk, *Planet Space Sci* **53**, 413–421 (2005)  
J. Jones, W. Jones, *Mon. Not. R. Astron. Soc.* **367**, 1050–1056 (2006)  
J. Jones, A.R. Webster, W.K. Hocking, *Rad. Sci.* **33**, 55–65 (1998)  
T.J. Jopek, G.B. Valsecchi, Cl. Froeschle, *Mon. Not. R. Astron. Soc.* **304**, 751–758 (1999)  
D.W.R. McKinley, *Meteor Science and Engineering*. (McGraw Hill, 1961)  
G.B. Valsecchi, T.J. Jopek, Cl. Froeschle, *Mon. Not. R. Astron. Soc.* **304**, 743–750 (1999)  
F. Verniani, *J. Geophys. Res.* **78**, 8429–8462 (1973)  
A.R. Webster, P.G. Brown, J. Jones, K.J. Ellis, M. Campbell-Brown, *Atmos. Chem. Phys. Discuss* **4**, 1181–1201 (2004)  
R.J. Weryk, P.G. Brown, *Comparisons of Simultaneously Detected Electro-optical and Radar Meteors, Meteoroids2007*. (Barcelona, 2007) this issue